

Novel Vapor Chambers for Heating and Cooling of Advanced Sorption Systems

Haley E. Myer[1] and Michael C. Ellis[2]
Advanced Cooling Technologies, Lancaster, PA, 17602

The Carbon Dioxide Removal Assembly (CDRA) on the International Space Station (ISS) uses a zeolite material to remove respirated CO_2 from cabin air. The zeolite material, a porous ceramic with low thermal conductivity, selectively adsorbs and desorbs CO_2 most efficiently at specific temperatures. This requires a full-scale thermal management system to heat and cool the zeolite for adsorption and desorption stages. NASA's current state-of-the-art thermal management system utilizes cartridge heaters encased in aluminum, star-shaped fins, which are distributed throughout the zeolite bed for heating. Cabin air is blown through the zeolite bed for cooling. This design presents many challenges, including nonuniform zeolite bed temperature, slow heating and cooling rates, and separate heating and cooling modes. Under a NASA SBIR Phase I program, Advanced Cooling Technologies designed, fabricated, and tested a prototype, titanium-water vapor chamber that improves on the current CDRA state-of-the-art thermal system. The developed vapor chamber combines the heating and cooling systems into one thermal management device, reducing overall system size, weight, and power of the CDRA. Testing of the vapor chamber demonstrated a 6x greater initial sorbent bed cooling rate, a 16% increase in maximum average sorbent bed temperature, and a 17% improvement in time to reach steady-state compared to the current state-of-the-art. Additionally, ACT demonstrated successful printability of the titanium, star-shaped vapor chamber, and the vapor chamber maintained structural integrity while operating under the high pressures of a saturated working fluid.

Nomenclature

ACT	=	Advanced Cooling Technologies, Inc.
AM	=	Additive Manufacturing
CDRA	=	Carbon Dioxide Removal Assembly
CNC	=	Computer Numerical Control
DMLS	=	Direct Metal Laser Sintering
ECLS	=	Environmental Control and Life Support
ISS	=	International Space Station
SOTA	=	State-of-the-art
SWaP	=	Size, Weight, and Power
TC	=	Thermocouple
VC	=	Vapor Chamber
D_v	=	Hydraulic Diameter
h_g	=	Heat of Fusion
ρ	=	Density
μ	=	Dynamic Viscosity
σ	=	Surface Tension
θ	=	Wetting Angle

[1] R&D Engineer, Advanced Cooling Technologies, 1046 New Holland Ave Building 2, Lancaster, PA 17601
[2] Senior R&D Engineer, Advanced Cooling Technologies, 1046 New Holland Ave Building 2, Lancaster, PA 17601

I. Introduction

TO improve upon the current state-of-the-art (SOTA) thermal management system for the CDRA zeolite bed, Advanced Cooling Technologies, Inc. (ACT), designed, fabricated, and tested a star-shaped, additively manufactured (AM), titanium-water vapor chamber prototype. This prototype would replace the cartridge heater and aluminum fin design currently used to heat the zeolite material in the Carbon Dioxide Removal Assembly (CDRA) on the International Space Station (ISS). The CDRA is a subassembly of the Environmental Control and Life Support (ECLS) system on the ISS. The primary function of the CDRA is to remove CO_2 from cabin air. This is accomplished using a sorbent material, zeolite, to adsorb and desorb CO_2. Images of the CDRA system can be found readily in the literature. Zeolite has a highly porous molecular structure, and CO_2 can favorably bond within these pores at certain temperatures and pressures. This molecular bonding process is exothermic during CO_2 adsorption and endothermic during CO_2 desorption. Thus, the zeolite material on the CDRA must be heated and cooled to very specific temperatures for effective desorption and adsorption of CO_2, respectively. The current CDRA operates most effectively when the sorbent bed is cooled to 20°C for adsorption and heated to 220°C for desorption. ACT's proposed thermal management system is designed to heat and cool the zeolite to these specific temperatures at faster rates than the SOTA design, with additional benefits such as reduced overall system size, weight, and power (SWaP) and adaptability to future sorbent materials.

Figure 1 illustrates the designed full scale thermal management system, which utilizes an array of two-phase vapor chambers to uniformly heat and cool the zeolite bed. The vapor chambers run parallel and connect to a heating source and a cooling source on opposite ends. This combines the heating and cooling mode of the thermal management system, which is an improvement in SWaP over the current SOTA thermal management system. The current NASA SOTA thermal management system for the CDRA utilizes cartridge heaters and aluminum fins to heat the sorbent bed and cooling channels to cool the bed. This system relies solely on conduction to spread heat from the cartridge heater to the bed. Additionally, it takes up considerable SWaP since the heating and cooling modes are separate. By utilizing a vapor chamber, ACT can make considerable improvements over the current NASA SOTA design in each SWaP, temperature ramp-up rates, and temperature uniformity of the sorbent bed.

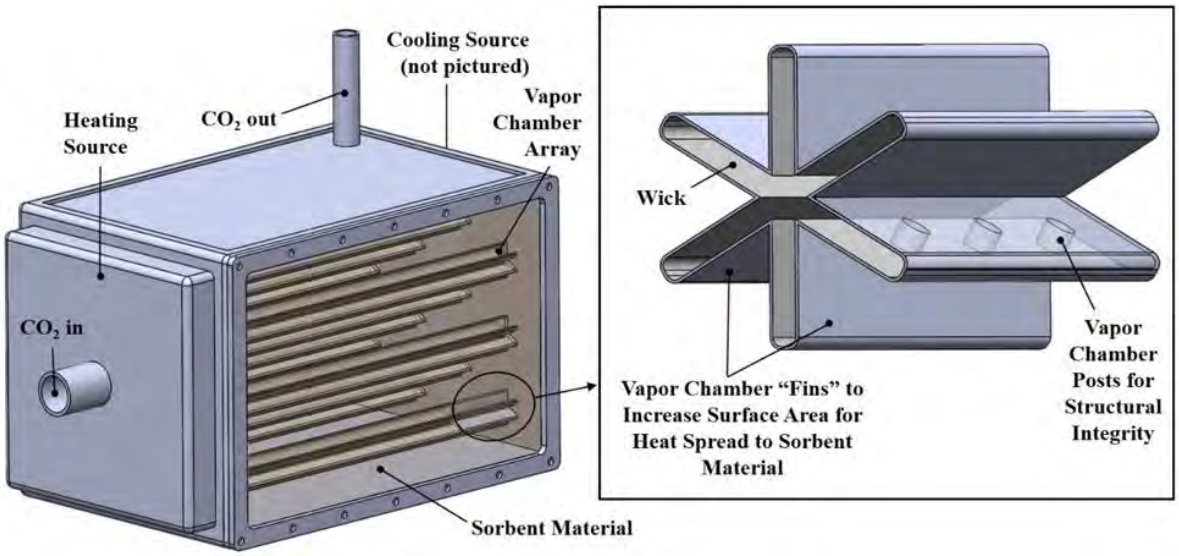

Figure 1. *ACT's full scale bed design for effective heating and cooling of sorbent material. The vapor chambers are hexagonally arranged through the bulk of the zeolite material.*

Vapor chambers are able to transport high amounts of power by taking advantage of two-phase heat transfer. Figure 2 illustrates the heat flow through the vapor chamber in both heating and cooling mode. In heating mode, heat is applied at the evaporator, and the liquid in the evaporator turns to vapor, storing its latent heat of vaporization in the process. The vapor will travel down the length of the vapor chamber due to the temperature gradient and thus pressure gradient along the length. The vapor will condense on the walls of the vapor chamber touching the sorbent bed, since this is the coolest part of the system. When the vapor condenses, it releases its latent heat of vaporization. This heat

will conduct through the thin titanium walls and into the sorbent bed. The liquid will return to the evaporator through the wick via capillary action, where the process will repeat itself. When in cooling mode, the concept is the same, except now the sorbent bed area becomes the evaporator, and the flanged end with coolant flow becomes the condenser. The heat from the sorbent bed will heat the liquid in the wick, causing it to evaporate and store its latent heat of fusion. The vapor will travel to the flanged end of the vapor chamber, now the coldest area due to coolant flow, where the vapor will condense into liquid and release its heat to the coolant. The liquid will return to the sorbent bed area via capillary action. The wick is not direction-dependent since the functioning of the liquid flow relies on capillary pressure. Thus, the vapor chamber is able to function in both heating and cooling modes as described. This reduces the size, weight, power usage, and cross-sectional area of the vapor chambers compared to the state-of-the-art cartridge heater and fin and convective cooling design.

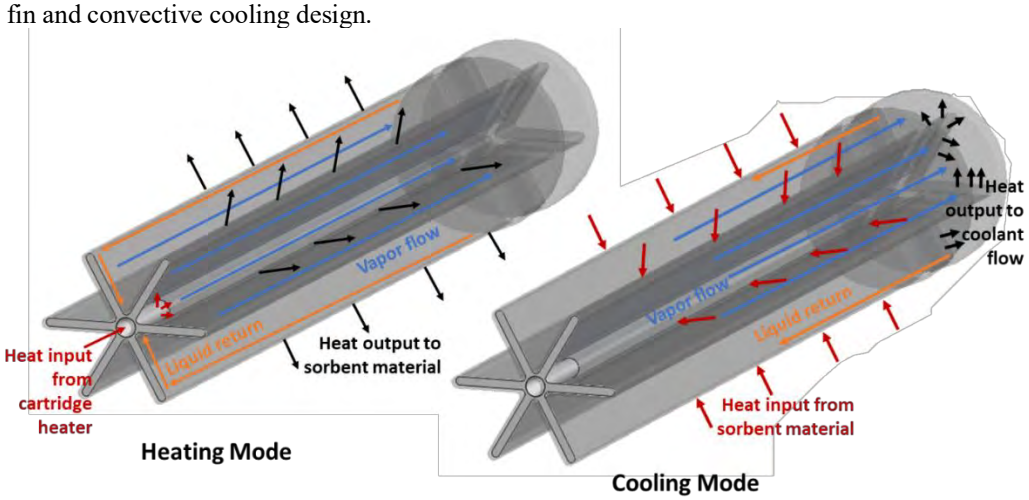

Figure 2. *Schematic to visualize heat and vapor flow in the proposed vapor chamber design while in heating and cooling mode.*

ACT has designed, fabricated and tested a prototype vapor chamber to demonstrate a well-rounded thermal improvement over the SOTA cartridge heater and aluminum fin design. The development of the prototype and testing results are shared in this paper.

II. Vapor Chamber Design

The vapor chamber grooves were designed for optimized power capacity of the device, and the vapor chamber posts were designed for structural integrity at high pressures. The structural posts traverse the grooves to not hinder liquid flow. The grooves allow the vapor chamber to carry water back to the evaporator via capillary action once it condenses. To arrive at the optimal groove geometry, the maximum developed capillary pressure, the vapor and liquid pressure drop, and the viscous limit for the operating range of the vapor chamber were calculated. Also, a test piece was made to ensure sufficient wettability between water and titanium. The maximum capillary pressure must be above the total liquid and vapor pressure drop for the vapor chamber grooves to function. Otherwise, dry out will occur, and the vapor chamber will not be able to transport power via two-phase heat transfer. Various groove heights, groove widths, and groove thickness geometries were explored. The results for the finalized geometry of maximum capillary pressure and total pressure drop are shown in Figure 3, along with the equations used for the calculations.

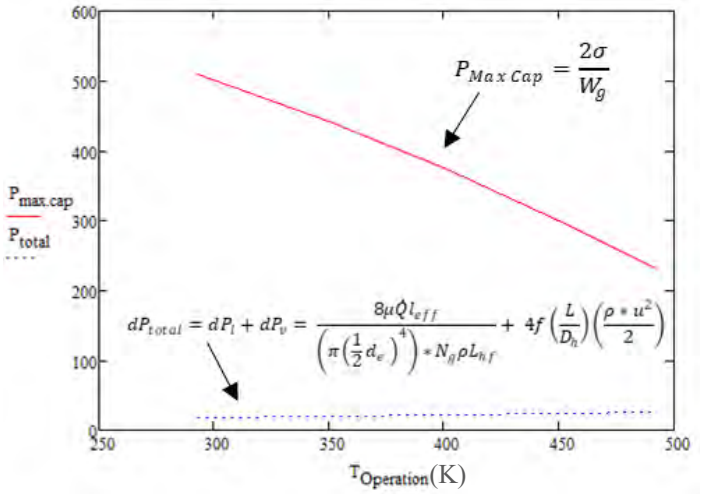

Figure 3. *Maximum capillary pressure and total pressure drop over the vapor chamber operating temperature range.*

Next, the viscous limit was calculated, to ensure there will be a high enough pressure drop at the low end of the temperature operating range to move the vapor along the length of the vapor chamber. The viscous limit equation for grooves is $Q_{max,visc.} = {D_v}^2 h_g \rho_g \rho_l / 64 * \mu * l_{eff}$, where D_v is the hydraulic diameter of the vapor space, h_g is the heat of fusion, ρ_g and ρ_l is the density of gas and liquid, μ is the dynamic viscosity of the liquid, and l_{eff} is the effective length. A total of 24 W is needed by one of the designed vapor chambers to heat a unit cell of zeolite in the full-scale design. Thus, the device will not reach its viscous limit until around 5°C, so it will function in this application.

A groove study was completed to demonstrate the selected groove sizes were printable, and the wettability of titanium was sufficient with water for the designed grooves. A test piece the length of the final device was additively manufactured out of titanium via direct metal laser sintering (DMLS) with 4 different groove widths, and 3 grooves for each width. The piece was placed horizontally in distilled water, and the height of wicking of each of the grooves was recorded. Then, the wetting angle of water and titanium was calculated based on this wicking height using Equation 1, where h is the wicking height, σ is the surface tension of water, D is the depth of the groove, W is the width of the groove, θ is the wetting angle, ρ is the density of water, and α is the angle of the groove away from vertical.[2]

$$h = \frac{\sigma[(2D + W)\cos(\theta) - W]}{\rho g D W sin(\alpha)} \quad (1)^2$$

The results for the average wicking height and wetting angle are recorded in Table 1. Upon optical microscopy inspection, it was observed that Groove No. 2 and 4 had areas where the wall collapsed, thus these geometries were not selected. Groove 1 geometry was chosen for the prototype due to its good printability and acceptable wetting angle. A visual image of the wettability test as well as a microscope image of the final selected Groove 1 geometry are shown in Figure 4.

Table 1. *Analytical results of wettability testing.*

Groove No.	Groove Width (in)	Avg. Wicking Height (mm)	Corresponding Wetting Angle (deg)
1	0.023	4.064	81.94
2	0.011	5.997	78.058
3	0.027	3.175	83.711
4	0.014	4.763	80.54

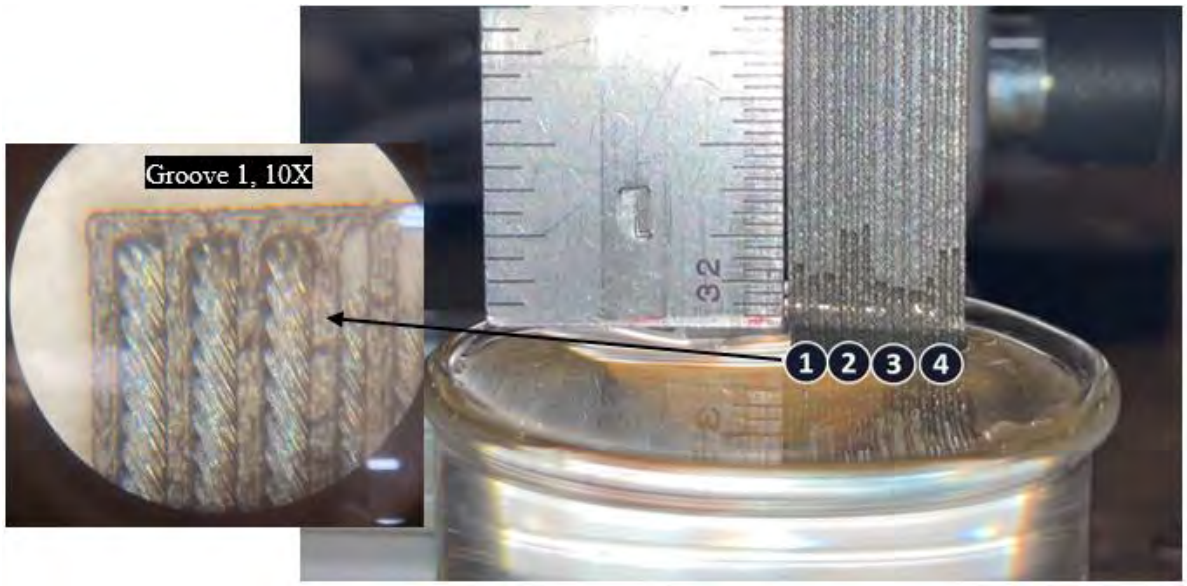

Figure 4. *Visual results of wettability testing (right) and groove surface roughness under a microscope (left).*

An iterative structural design study was completed in Solidworks to design the posts of the vapor chamber. The posts are X-shaped for printability in the vertical direction. The posts sit on top of the grooves, so they do not hinder liquid flow. The final vapor chamber will be filled with saturated water, which has a saturation pressure of 313 psi at a temperature of 220°C, which is the max operating temperature of the vapor chamber. A factor of safety of 3 was targeted and achieved for the structural design. Powder removal holes, fill holes, and flanges for fitting into the test apparatus were added to the design. Figure 5 illustrates the design of the posts in the vapor chamber with printing considerations.

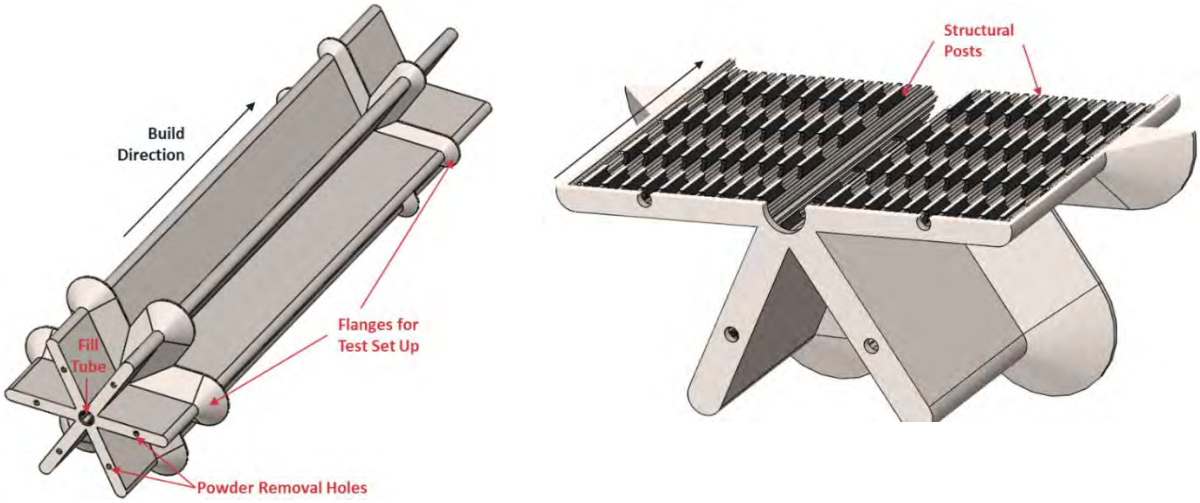

Figure 5. *Section view illustrating post design (right) and printing considerations for vapor chamber (left).*

III. Fabrication of Vapor Chamber and Test Bed

The designed vapor chamber was printed out of Ti-64 via direct metal laser sintering (DMLS) in the vertical direction. The printed vapor chamber is shown in Figure 6. Upon arrival, ACT placed the vapor chamber in an 8-hour acetone bath, with manual agitation every hour, and then a 16-hour acetone bath with manual agitation at the end.

Then, the vapor chamber was flushed with methanol through the fill tube hold. Next, the powder removal holes were welded shut and a fill tube with a valve was welded on to the center hole.

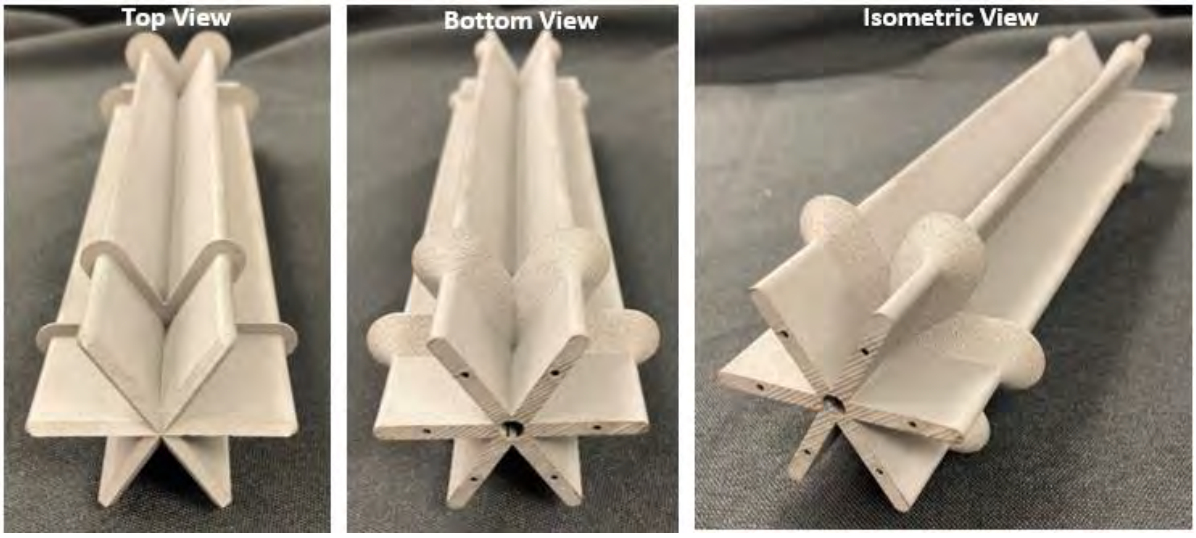

Figure 6. *Additively manufactured vapor chamber.*

In addition to the vapor chamber, ACT fabricated a replica of the NASA SOTA cartridge heater and fin design for a baseline comparison in test data. This was CNC machined out of Al-6061, and the fins follows the geometry of the NASA SOTA design with no taper along the length.[1] The SOTA replica is shown in Figure 7.

For the purposes of testing at this phase, a demonstration of improved heating and cooling times of the vapor chamber compared to the NASA SOTA is desired. Thus, a subscale zeolite test bed was constructed with 15 probe thermocouples to record temperatures throughout the bulk of the zeolite bed. 16 surface thermocouples were also mounted on the surface of each device, located halfway between the center and tip of the fins. The placement of the thermocouples is detailed in Figure 8. The placement allows validation of both radial and lateral isothermality of the device. The same test bed was used for testing both the vapor chamber and the NASA SOTA replica.

The test bed was constructed out of stainless steel and is shown in Figure 79. The bed is bolted together with silicone gaskets, and the bed includes two air inlet and two air outlet manifolds. The probe thermocouples enter the bed with fittings, and the surface thermocouples exit the bed in a hole sealed with RTV silicone. The bed is filled with Zeolite 13X beads via the snowstorm technique.[3]

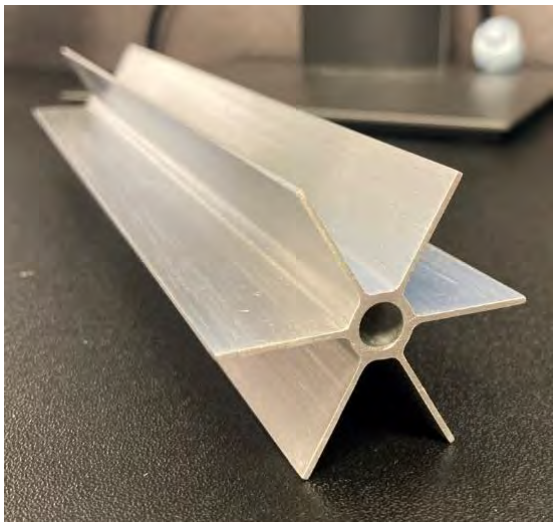

Figure 7. *NASA SOTA cartridge heater and fin design replica for baseline testing***.**

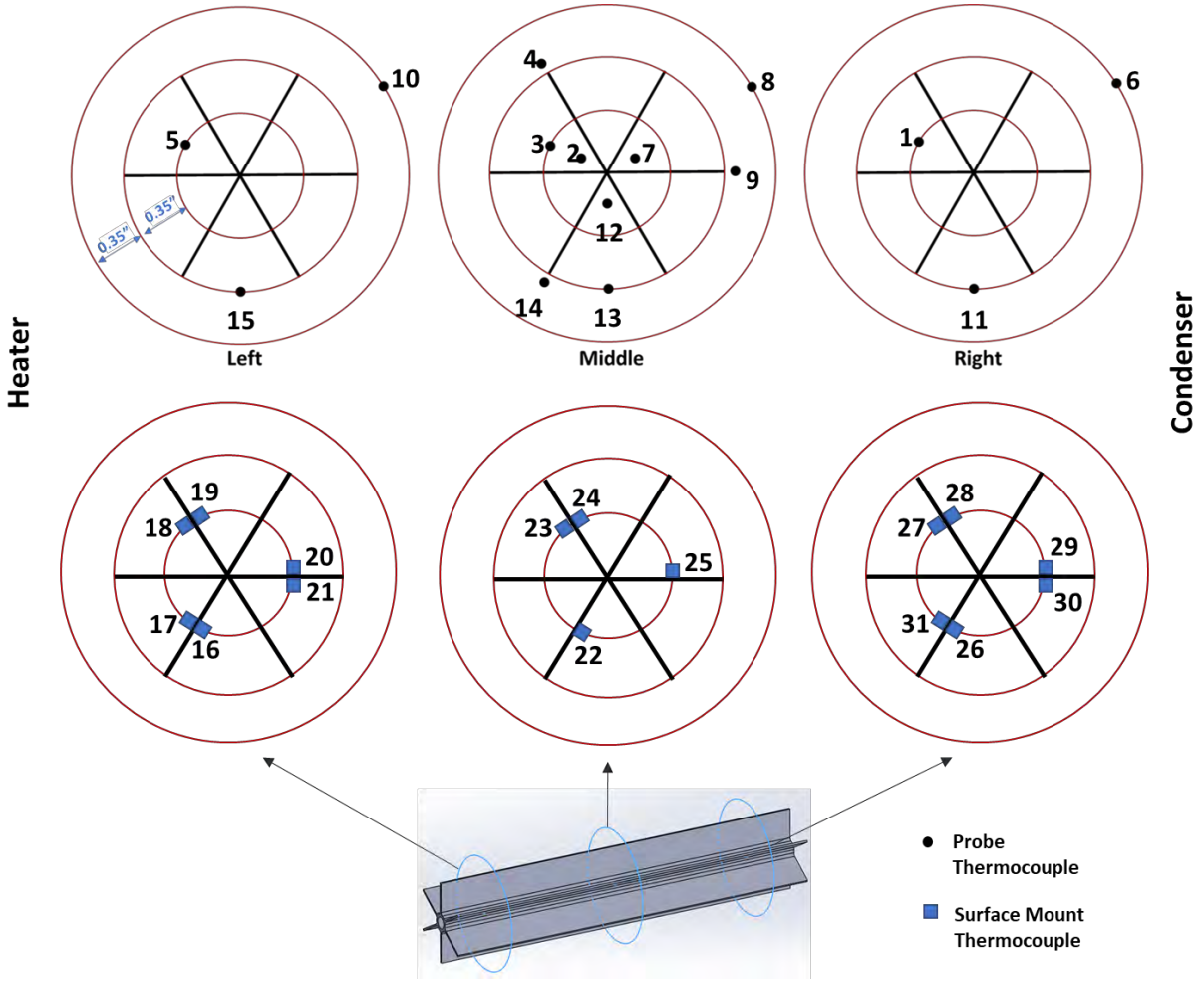

Figure 8. *Location of thermocouples throughout zeolite test bed.*

The vapor chamber was charged through the fill tube with water as a working fluid prior to testing. Adhesive heaters were secured and clamped around the evaporator and heated to 150˚C. Surface thermocouples were placed near the evaporator and condenser and monitored as the adhesive heaters increased in temperature and reached steady state. After experimenting with various fluid charge amounts, it was determined that 15 grams is the ideal charge. This charge maintains the tightest tolerance in temperature, only about 1˚C when vertical, between the evaporator and condenser.

The vapor chamber was flipped horizontally and vertically 2 times each with the heaters on. The temperature difference between the condenser and evaporator is recorded in Figure 10. The vapor chamber maintained less than a 1.5°C difference in temperature between the evaporator and condenser regardless of orientation. The tight temperature tolerance when the vapor chamber is oriented horizontal – only about 1°C – also indicates there is no puddle flow in the vapor chamber. This is an almost 16°C improvement in isothermality over the NASA SOTA design, as illustrated by the test data shown in Figure 11. In this

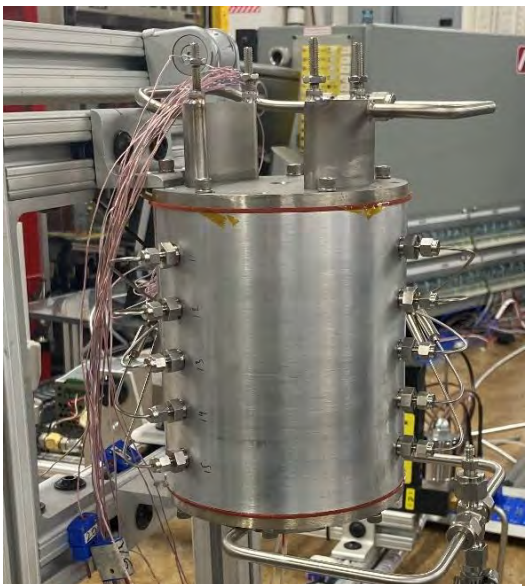

Figure 9. *Constructed zeolite test bed used for NASA SOTA and VC testing.*

NASA SOTA test, both the cartridge heater for the aluminum extrusion and the adhesive heaters for the vapor chamber were run from idle to a constant temperature of 150°C. Insulation was put on the exterior of both the vapor chamber and solid aluminum star for the test. The temperature difference from the evaporator to condenser is 16°C higher initially in the aluminum extrusion, and 3°C higher at steady state than the vapor chamber at steady state. Additionally, the vapor chamber reaches steady state almost instantly (50 seconds), whereas the aluminum extrusion does not reach steady state until about 850 seconds into the test, or about 15 minutes, which is a 17% improvement in time to reach steady state.

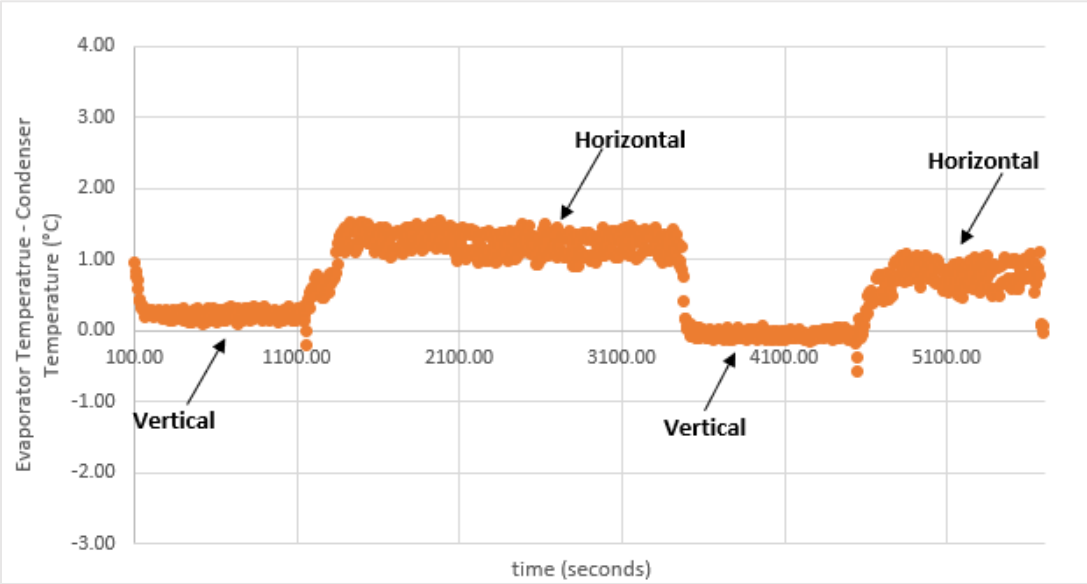

Figure 10. *Data for the temperature difference between the evaporator and condenser of the vapor chamber in both vertical and horizontal orientations*

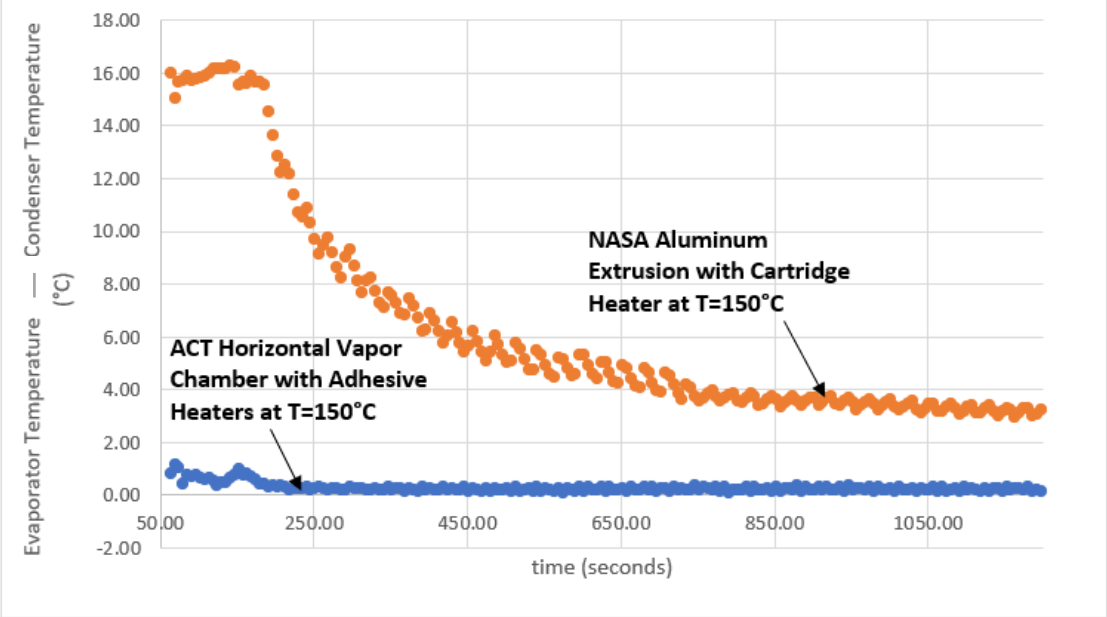

Figure 11. Data for the temperature difference from evaporator to condenser of the NASA aluminum extrusion with cartridge heater at T=150°C and the ACT vapor chamber with adhesive heaters at T=150°C.

IV. Prototype Testing and Results

Heating mode and cooling mode tests were run for both the vapor chamber and the aluminum star extrusions. For both thermal management devices, a dewar of Praxair Ultra Zero air was used for testing to ensure no water vapor or oil contaminants were in the air flow stream. An air flow rate of 1.5 L/min was used for every test. Rope heaters were placed on the air inlet tubes to provide a preheat of 80°C upon entry for every single test, except for the ACT vapor chamber cooling mode tests. The power was varied in the horizontal orientation from 15 to 40W in 5W increments for both devices. Although the target ramp-up time for the bed is around 80 minutes, each test was run for 120 minutes to collect more data on the thermal management devices. The results for the horizontal heating 40W tests are shown in Figure 12 to Figure 15.

Figure 12 shows the results for thermocouples (TC's) 19, 24, and 28, which are on the surface of both devices (reference Figure 8 for thermocouple locations). The respective vapor chamber TC's are approximately 20°C hotter than the NASA SOTA device after 3600 seconds. In addition, the vapor chamber is much more isothermal laterally than the NASA SOTA, which has a temperature difference of 16°C from end to end.

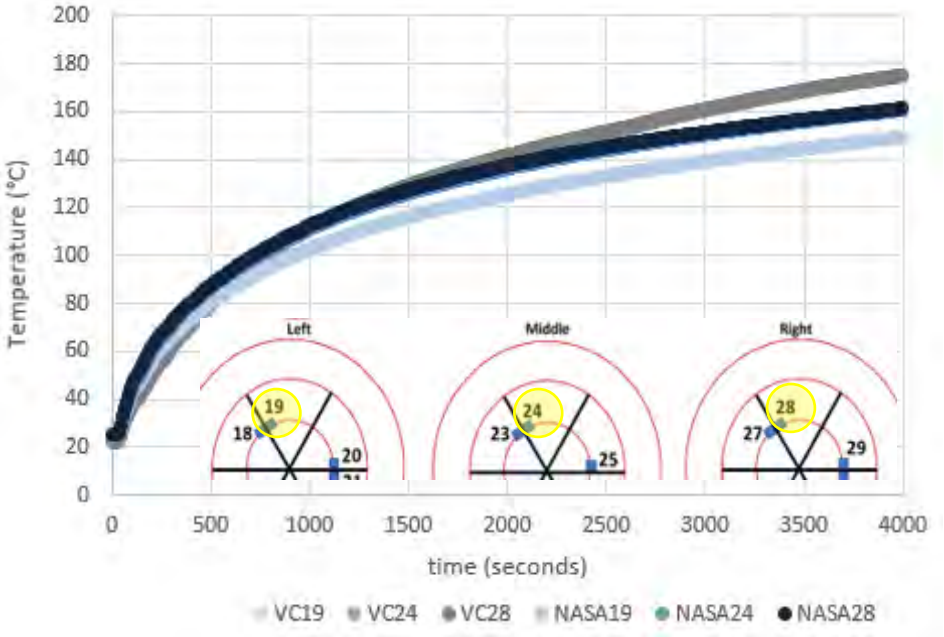

Figure 12. *Results from 40W test for surface thermocouples 19, 24, and 28.*

Figure 13 shows the results from the 40W test for TC's 2, 7, and 12, closest to the center of the devices. Both the vapor chamber and the NASA SOTA show good radial isothermality throughout the 3600 seconds heating period. The zeolite closest to the vapor chamber, though, is 7°C hotter than the zeolite beads closest to the NASA SOTA after heating for 3600 seconds.

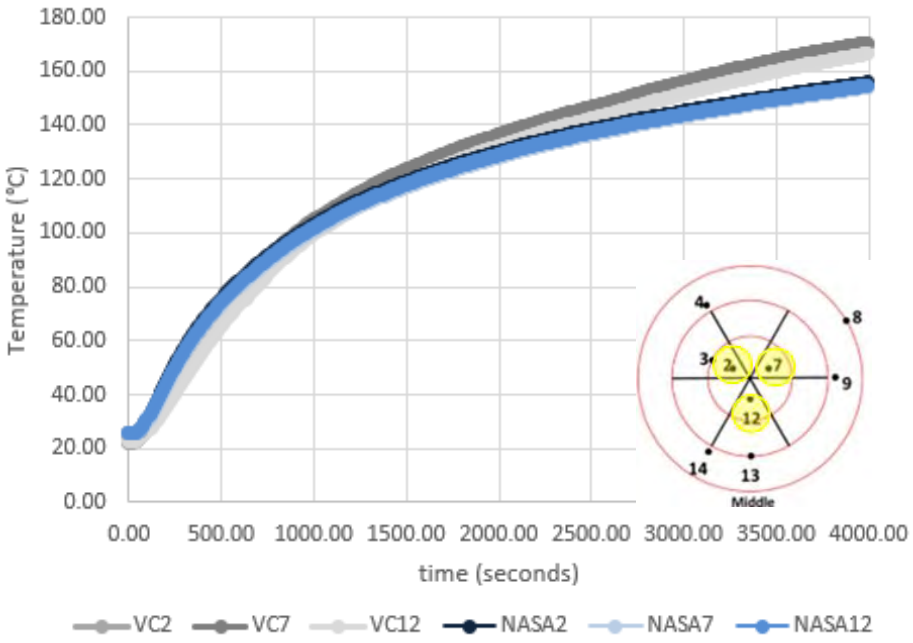

Figure 13. *Results from 40W test for probe thermocouples 2, 7, and 12.*

Figure 14 shows the results from the 40W test for TC's 1, 3, and 5. While the vapor chamber is hotter than the NASA SOTA at 3600 seconds, there is an anomaly with TC 3. It is expected this middle TC is cooler than TC's 1 and 5 because the vapor is not condensing in the middle of the device. This will be mitigated in the Phase II with the improved wick design. However, it can be seen that without this anomaly, the vapor chamber is more isothermal laterally than the NASA SOTA.

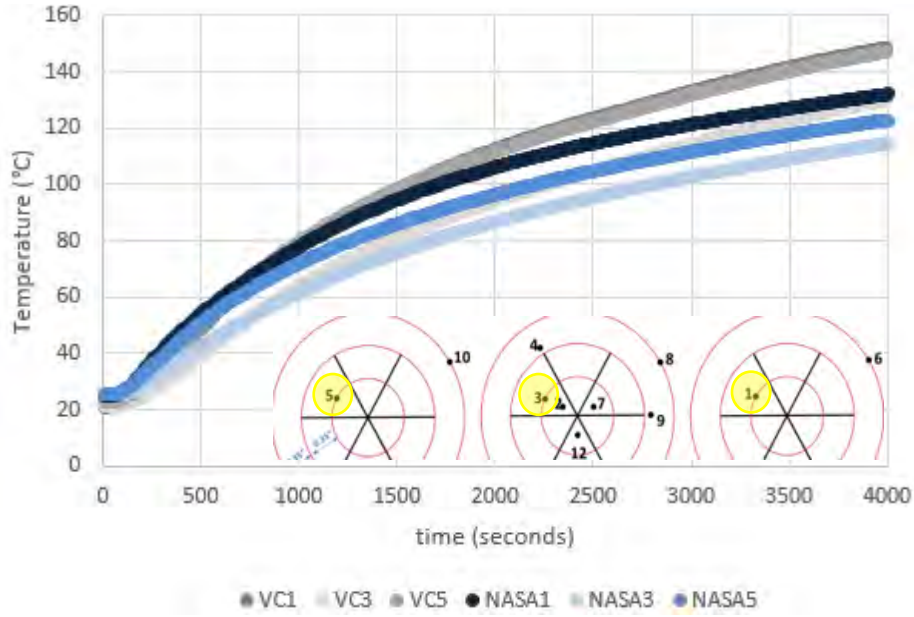

Figure 14. *Results from 40W test for probe thermocouples 1, 3, and 5.*

Figure 15 shows the results from the 40W test for TC's 6, 8, and 10. The vapor chamber, at these probe thermocouples 0.70" away from the center of the devices, are 11°C hotter than the NASA SOTA after 3600 seconds. This is a promising results to show that even with the extremely low thermal conductivity of the sorbent being the main obstacle

to moving heat throughout the device, the vapor chamber is still able to heat the furthest TC's hotter than the NASA SOTA device, proving the device can overcome the poor thermal conductivity of the sorbent bed.

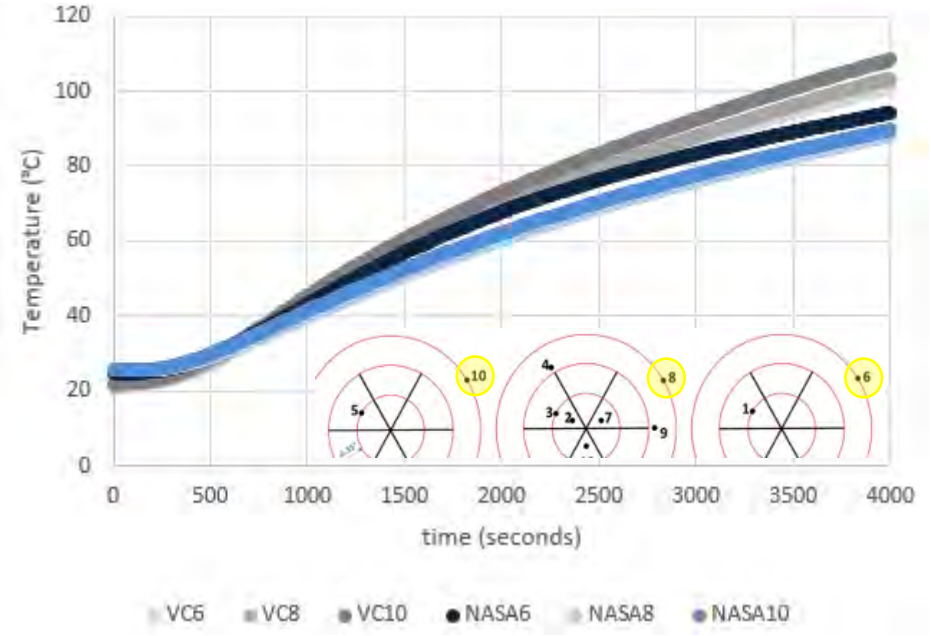

Figure 15. *Results from 40W test for probe thermocouples 6, 8, and 10.*

Next, the vapor chamber was tested in cooling mode. In the vapor chamber cooling test, the vapor chamber was heated at 70W for 9000 seconds with air flow through the bed at 1.5 L/min. Then, the heaters were shut off, and chilled water at 5°C and 5 L/min was flown through the cooling manifold over the condenser end of the vapor chamber. This simulates the water from the low temperature loop on the ISS. A baseline test was run for comparison, where 70W was applied to the heaters for 9000 seconds with air flow through the bed at 1.5 L/min (same as prior test). Then, the heaters were turned off, with air still flowing through the bed, and the bed was allowed to air cool convectively.

The results for both tests for the center thermocouples closest to the vapor chamber (2, 7, 12) are shown in Figure 16. The results for both tests for the thermocouples farthest from the vapor chamber (6, 8, 10) are shown in Figure 17. For thermocouples 2, 7, and 12, the vapor chamber cooled zeolite beads cool in ~8 minutes from 180°C down to 60°C, while in the same time, the air-cooled zeolite beads only cool from 180°C to 160°C. This is an initial cooling rate of 15°C/min with the vapor chamber, compared to only a 2.5°C/min without the vapor chamber. This is a 6x greater initial cooling rate with the vapor chamber versus without it. For the overall cooling period, the average cooling rate with the vapor chamber is 1.19°C/min, while without it is only 0.99°C/min – a 20% improvement in average cooling rate with the vapor chamber. An even more promising result is for thermocouples 6, 8, and 10, which are situated 0.75" away from the center of the vapor chamber. There is still a substantial increase in cooling rate with the vapor chamber. For the entire cooling period, the average cooling rate with the vapor chamber is 0.76°C/min, and without the vapor chamber it is only 0.56°C/min. This is a 36% increase in average cooling rate with the vapor chamber, for the zeolite beads farthest away from the cooling device. Not only does the vapor chamber combine the heating and cooling modes of the thermal management system, but it also offers an improvement in the average cooling rate for the entire zeolite bed compared to the current state of the art.

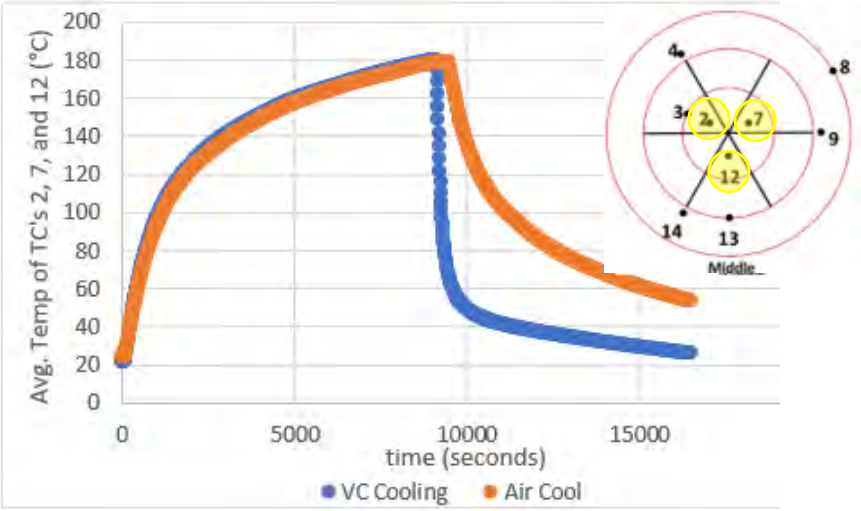

Figure 16. *Cooling data for thermocouples 2, 7, and 12 for vapor chamber versus air cool.*

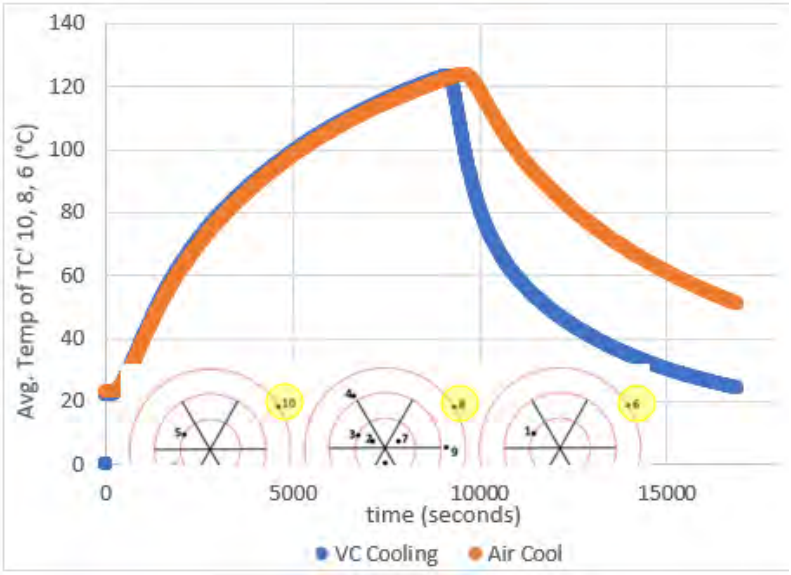

Figure 17. *Cooling data for thermocouples 6, 8, and 10 for vapor chamber versus air cool.*

V. Conclusion

Overall, the ACT vapor chamber demonstrated an increased cooling rate, increased heating rate, improved time to reach steady state, lower size, weight, and power, and improved future adaptability of the vapor chamber compared to NASA's current state-of-the-art cartridge heater and aluminum fin design. Specifically, ACT's vapor chamber offers a 6x greater initial sorbent bed cooling rate as opposed to cooling with air flow through the sorbent bed. Additionally, ACT demonstrated the vapor chamber has a 17% improvement in time to reach steady state compared to the current cartridge heater and aluminum fin design. There is also a 16% increase in maximum average sorbent bed temperature after 1 hour of heating at 40W with the vapor chamber compared to the NASA aluminum fin design. Lastly, the titanium vapor chamber was successfully additively manufactured, and the device hermetically withstood

the pressures of operation at 200°C. This manufacturing success, along with the vapor chamber device combining heating and cooling modes, provides great adaptability to future designs.

Acknowledgments

ACT would like to acknowledge Max Demydovych and Megan Gettle for their support in the design, fabrication, and testing efforts in this project. ACT would also like to acknowledge the NASA SBIR program for financially supporting the project, and Tra-My Justine Richardson for her technical support and guidance as the technical monitor.

References

[1]Schunk et. al. [2017]. Four Bed Molecular Sieve – Exploration (4BMS-X) Virtual Heater Design and Optimization.
[2]Abadi, G. and Bahrami, M. [2020]. A General Form of Capillary Rise in Microgrooves. *Scientific Reports.*
[3]F. Safranyik, et. al., [2020]. Optimal and Effective Technique for Particle Packing. *Advanced Powder Technology.* 31 (8).